Determination of the Rocking Curve and Reflection Efficiency of a Quartz Crystal X-ray Imager

Thesis

Presented in Partial Fulfillment of the Requirements for Graduation with Research Distinction in Physics in the Undergraduate Colleges of The Ohio State University

By:

Perrin Schiebel

Project Advisor:

Dr. Richard R. Freeman, Department of Physics

Abstract

A spherically curved Bragg crystal was characterized for use in experiments utilizing the Kα emissions of higher Z materials than current crystals allow. The National Synchrotron Light Source at Brookhaven National Laboratory was used to study the crystal with x-rays of energies 15.6909 keV, 16.5210 keV, 17.4793 keV, and 22.1629 keV corresponding to Zr $K_{\alpha 2}$, Nb $K_{\alpha 2}$, Mo $K_{\alpha 1}$ and Ag $K_{\alpha 2}$ emissions, respectively. The crystal was then used to image the Kα emission from a Zr target irradiated using the multi-terawatt laser at the University of Rochester. In conclusion the crystal was a successful diagnostic, and provided the first ever image of Zr Kα radiation.

Table of Contents

List of Figures

Introduction

X-rays are a useful tool in many experiments as they are energetic enough to penetrate many materials, but not so energetic that they pass through without providing any information. However, they also provide difficulties in terms of imaging, as conventional light imaging tools such as metallic mirrors are unable to image these higher energies.

Bragg crystals are extremely useful tools in the characterization of x-rays. They are extremely sensitive to the angle of incident radiation, even to the range of micro radians. In relation to this characteristic they are able to distinguish energies of incident radiation. Flat Bragg crystals may therefore be used in x-ray spectroscopy, whereas spherically curved Bragg crystals provide the ability to image an x-ray source.

Background

Electromagnetic radiation in the range of 120 eV to 120 keV, corresponding to wavelengths of 10 to 0.01 nm, is often utilized in science. This energy range, referred to as x-rays, has many uses. Some experiments will use x-rays produced by an x-ray source such as an x-ray tube or synchrotron to probe an object. Others may look at x-rays which are emitted from an object to gain information about it. These photons, while useful, also present some unique obstacles in terms of detection and interpretation. Their short wavelength prevents the use of conventional tools such as mirrors. One of the simple, yet powerful, tools in the study of x-rays is the Bragg crystal.

X-rays will scatter off of atoms or molecules in a crystal lattice. When a photon encounters an electron belonging to one of these atoms it will be absorbed and reemitted in a Thomson scattering process. This process is elastic and as such the x-rays propagating away from the crystal are the same energy as the incident photons. Photons will interact with atoms in different planes of the lattice, and this will result in interference effects as shown in Figure 1.

a. b.

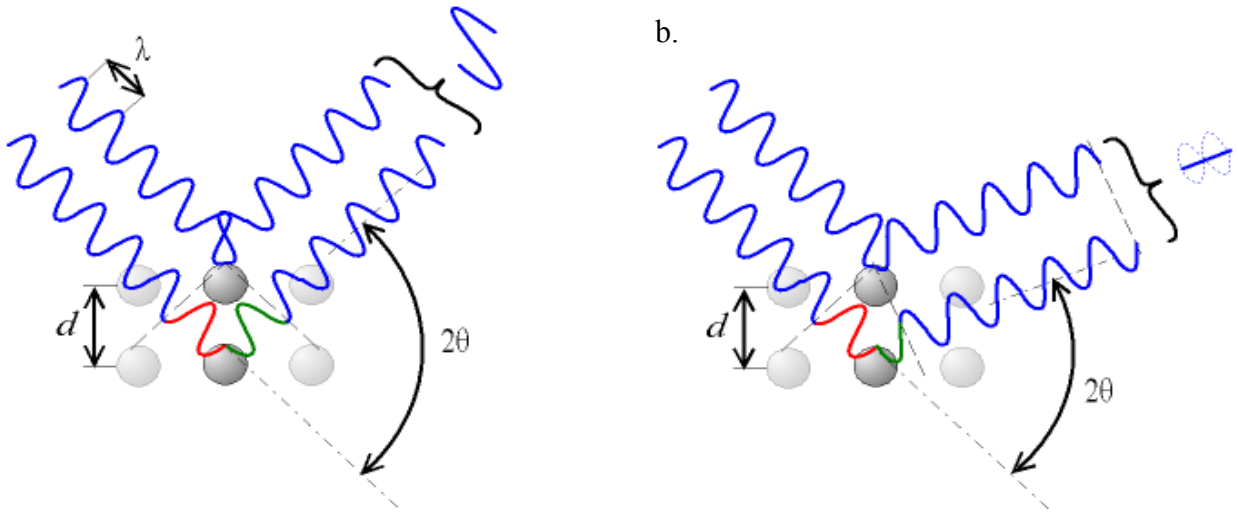

Wikipedia.org/wiki/File:Braggs_Law.svg

Figure 1. a) Constructive interference at the Bragg angle. b) Destructive interference where Bragg condition not met.

These effects are described by Bragg's Law

$$n\lambda = 2d\sin\theta$$

where n is an integer, usually interest lies in first order interference and n=1, λ is the wavelength of the x-ray, d is the spacing between planes in the crystal lattice, and θ is the compliment to the angle of incidence of the wave on the crystal. There is an angle, referred to as the Bragg angle,

which corresponds to the conditions for completely constructive interference. This angle is unique to any given d-spacing and x-ray energy.

In order to make experimental use of a crystal one much know the d-spacing, the reflection efficiency, and the rocking curve. The rocking curve refers to the range of angles for which the crystal will reflect a given wavelength. It is usually given as a full width at half maximum with the maximum being the point at which the Bragg condition is optimally met. The point at which the slope of the rocking curve is greatest is the point where intensity of the incident beam is reduced by half.

In order for the crystals to be accurate it is necessary for them have very limited flaws. For this reason materials such as Silicon are commonly used as the ability exists to make highly perfect Silicon crystals. The crystal used in this experiment is SiO_2, or quartz. These crystals are referred to as Bragg crystals solely based on their use in the diffraction of x-rays. They do not have any special properties that set them apart from other crystals. One simply takes advantage of the highly ordered nature of crystals and the fact that certain crystals are capable of diffracting x-rays to make clever use of them as a diagnostic tool.

There are two basic uses of Bragg crystals, illustrated in Figure 2. By using a flat crystal one can obtain the spectrum of an x-ray emitting source. Each unique wavelength being emitted will have a specific Bragg angle. Because the condition for completely constructive interference will be met at different angles for the different x-ray energies, the different wavelengths composing the beam will be separated. By reflecting the polychromatic light off of the crystal and to an imager it is possible to determine what energies are being emitted.

A spherical crystal will focus x-rays to create a real image. The process is like that of imaging using an ordinary metal mirror to reflect visible light. By simply placing the crystal in the path of the beam, x-rays which are either being emitted by an object or which have been generated to backlight an object will be reflected off of the crystal and on to an imaging device to obtain a picture of the object of interest. However, unlike an ordinary mirror, a crystal is used to image only a single wavelength, as all others will not meet the Bragg condition and will be rejected.

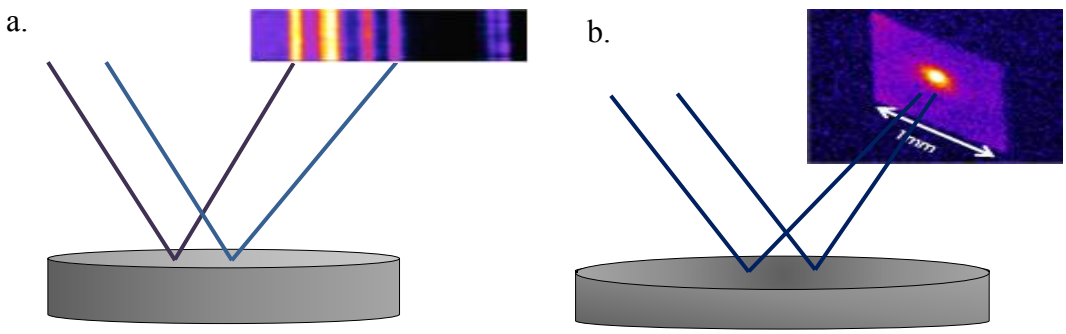

Figure 2. a) A flat crystal will separate energies in a polychromatic beam. b) A curved crystal will image a monochromatic beam.

The desired use of the Bragg crystal at the focus of this experiment is the study of high-energy (1-3 MeV) electrons generated by lasers interacting with matter, namely the electron yield and propagation. While studying these electrons directly is challenging, by taking advantage of Kα x-ray emissions the electron yield and divergence can be imaged using Bragg crystals.

When a laser with enough energy is incident on matter, it will strip electrons from atoms and accelerate them to high energies. The energetic electrons generated by the laser may then interact with bound electrons and eject the ground state electrons out of the atom. Ground state

electron vacancies in the atoms are filled by higher state electrons. When these higher state electrons relax to the lower energy they will emit a photon in the x-ray energy range. This radiation is referred to as Kα if the emitting electron comes from the L shell and Kβ if it is from the M shell, as depicted in Figure 3. The experiments of interest here use Kα, as this is a much more common occurrence than Kβ emission. The energy of these x-rays is in direct correlation to the element from which they are emitted. Elements with a higher Z will emit higher energies.

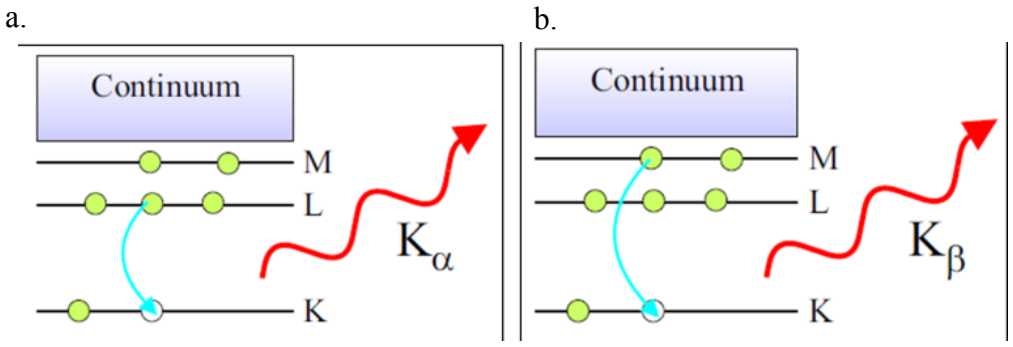

Figure 3. a) Kα x-ray released by L shell electron relaxing to the ground state. b) Kβ x-ray released by M shell electron relaxing to the ground state.

Using a spherical Bragg crystal these x-ray emissions can be imaged. In this experiment the crystal will be carefully aligned to the Bragg angle corresponding to the specific x-ray energy that the target metal produces. The x-rays will be diffracted off of the crystal and to a detector. In this way a real image of the emitted x-rays will be created.

These Kα emissions can be used to study electron propagation by using buried layers in flat targets. The targets are made of a material such as Aluminum, with buried fluorescent layers of metals such as Copper or Zirconium. The electrons generated when the laser interacts with the Al target will travel through the target. When they encounter the buried layer with a much higher

Z than Al, x-rays will be created which have enough energy to escape the target and be subsequently imaged. A schematic of this process is shown in Figure 4.

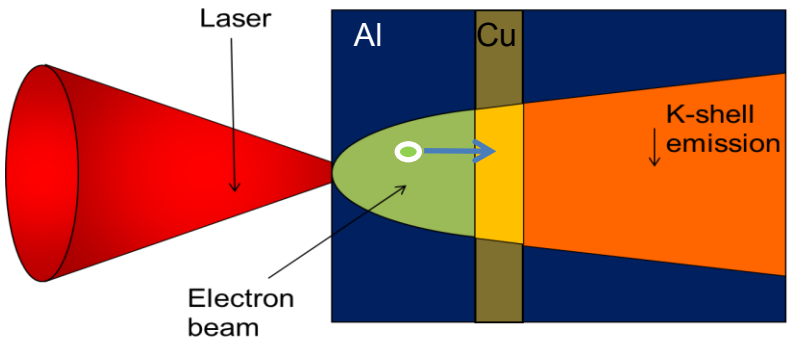

Figure 4. Flat target experiment. The laser strikes the Al target from the left producing electrons. Electrons encountering the Cu fluor layer produce Cu Kα x-rays.

The image created by the crystal is a picture of where the Kα came from, and in turn where the electrons were when they encountered the buried layer. The number of photons appearing in the image gives information about how many electrons traveled through the fluor layer. By performing the experiment a number of times with the fluor layer at different depths in the target, a picture of electron spot size and flux as related to target depth can be obtained. Combining this information gives a picture of how the electrons travel through the material, that is, how quickly the beam diverges and to what extent the electrons are attenuated.

These studies are crucial to the exploration of Fast Ignition, an approach to Inertial Confinement Fusion (ICF). The concept behind ICF is creating a fusion reaction by compressing the fusion components to extremely high densities. This may be accomplished using either direct or indirect drive. The chosen reaction for this process is deuterium-tritium (DT). In the direct drive approach, a spherical ablation shell of low-Z material surrounds either liquid or frozen DT and a core consisting of DT gas. Laser radiation will be applied to the shell from all directions,

causing the ablation layer to rapidly expand. Conservation of momentum forces the DT core to compress to extremely high pressures and temperatures where a central hot spot will ignite and the reaction will spread radially outward, burning through the fuel. This process is shown in Figure 5.

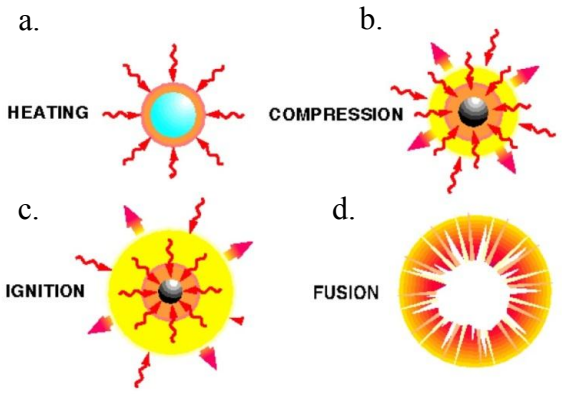

Figure 5. Direct drive fusion process. a. the ablative layer is heated evenly by long pulse lasers from all directions. b. The ablative layer expands away, causing the fuel to be compressed. c. A central hot spot will form and ignite the fusion reaction. d. The fusion reaction propagates through the fuel.

Indirect drive uses the same fuel capsule, but instead of heating the ablation layer directly using the lasers, the target is placed inside a hollow cone made of a high-Z material. Laser radiation will enter the cone and generate x-rays, in the same Kα process previously described, which are then responsible for the heating of the spherical shell. Because indirect drive requires the additional step of x-ray generation, direct drive is has approximately twice the gain.

However, direct drive suffers from major difficulties due to its sensitivity to variations within the beams used to compress the target, as well as any hydrodynamic instabilities in the fuel. Asymmetries in the implosion will cause waste of laser energy, and can prevent the fuel reaching densities which will ignite fusion. [1,2]

Fast ignition is a technique proposed to make direct drive more feasible. If successful it would allow the use of this more energy efficient mechanism while sidestepping some of the obstacles. The fast ignition technique involves inserting a gold cone in the target. A short pulse laser will be shot into the cone immediately after the long pulse lasers have compressed the target. Figure 6. is an illustration of this concept. The desire is that the short pulse laser will interact with the cone to generate a beam of high energy electrons. These electrons will propagate into the core and ignite the fusion process, allowing for more leeway in the restrictions on density. When the fuel is allowed to ignite spontaneously, the conditions in the core are that of equal pressure. However, by sending a beam of electrons to the core on a sufficiently short time scale the contents of the core can be viewed as being at equal density. In this model there is not a need for a hot spot at high peak density in order to start the reaction, and more of the mass will be at a lower peak density, allowing for a greater amount of the fuel to be utilized in the reaction. Fast ignition is a powerful concept, but one which relies entirely on a beam of high energy electrons, in the 1-3 MeV range, reaching the high-density core. [3]

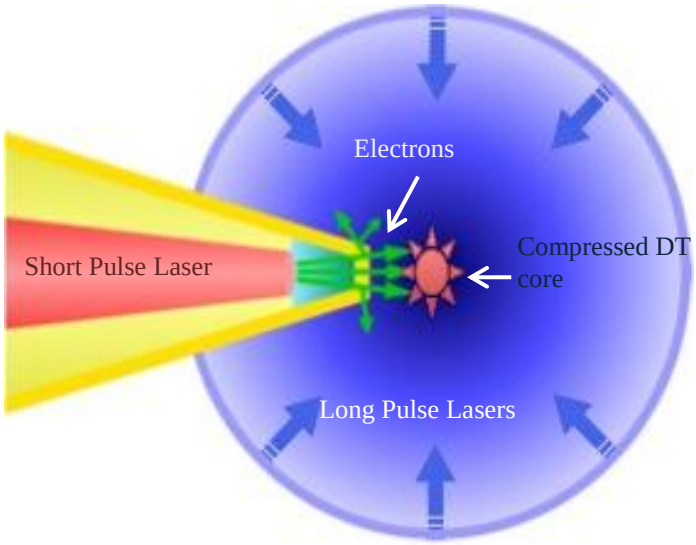

Figure 6. Long pulse lasers compress the target. A short pulse laser then generates electrons in a gold cone which will deposit their energy in the core to initiate the fusion reaction.

The properties of the interaction between high energy lasers and matter are not fully researched. It is unknown how electrons generated in these interactions propagate through matter. For fast ignition to work it is necessary that the electrons generated by the short pulse

laser travel in a collimated beam to the core of the target and deposit their energy there. Without knowing the characteristics of the electron beam, it is impossible to assess the feasibility of the fast ignition concept. Using the previously described experiments which utilize Bragg crystals to study the electrons accelerated by these high intensity (~10^{20} W/cm^2) lasers, it is hoped to determine to what extent the electrons travel in a collimated beam, and thus the viability of the fast ignition model.

Being able to successfully realize ICF is of great interest. As society's energy needs increase, it is necessary to find new means of generating energy. Fossil fuels are not going to be able to meet global energy needs for more than another century to two. Deuterium and tritium can be derived from water and lithium. These fuels are available anywhere in the world so there is the potential to greatly reduce the costs associated with transporting fossil fuels from extraction sites to power plants. The amount of energy per mass of this fuel is much greater than that for fossil fuels as well. One kilogram of DT can provide approximately as much energy as 10 million kilograms of fossil fuel. Additionally, the fuel itself does not become radioactive. The only radiation of concern is that of the components within the reactor, and those are safe for disposal after approximately one hundred years. [4]

Another positive asset to fusion energy is the fact that fusion does not create greenhouse gases. Coal power plants in the United States produce as much Carbon Dioxide as all of our vehicles combined. They also release sulfur dioxide and mercury into the environment. The only byproduct of fusion plants is a small amount of Helium, a noble gas which is released harmlessly into the atmosphere. [4] Fusion power plants would be much less harmful to the climate than current coal plants. [5]

Methods

In order for this crystal to be a useful diagnostic it was essential to know its properties. To characterize the quartz crystal it was necessary to use x-rays of well-known energy and flux. The crystal was taken to the National Synchrotron Light Source at Brookhaven National Laboratory in Upton New York. The X15A beamline was utilized as it is set up to provide photons of energies in the range of interest, namely those corresponding to the x-ray emissions of Zr $K_{\alpha 2}$, Nb $K_{\alpha 2}$, Mo $K_{\alpha 1}$ and Ag $K_{\alpha 2}$. These are of energies 15.6909 keV, 16.5210 keV, 17.4793 keV, and 22.1629 keV respectively.

The storage ring provides photons over a large range of energy, and a Bragg crystal monochromator was used to select photons of the desired energy. This monochromator operates via two flat crystals whose faces are parallel to each other. By rotating both crystals to the Bragg angle for the desired energy, the crystals will reflect only photons of that energy in a way that they carry on parallel to the original beam. By placing a small slit which will pass only these components parallel to the original beam all other energies will be trapped within the monochromator. In this case the slit was of width 1.6 mm and height 100 μm. This monochromator selects energies with a resolution of $\Delta E/E \sim 10^{-4}$. This means that all passed energy would be within 0.01% of the desired value.

An ionization chamber was used after the monochromator to provide information about the photon flux. This is accomplished via a box containing a gas as well as an anode and a cathode. The radiation will ionize particles in the gas or walls of the box. The ions and disassociated electrons will move due to the potential difference between the electrodes, and will travel to the electrode of opposite sign. This causes a small flow of current which is directly

proportional to the number of ions and thus the amount of incident radiation. This current may be measured and used to find the total flux of radiation. The total flux was found to be directly proportional to the electron current in the storage ring.

The crystal was mounted on a computer controlled goniometer with a total range of motion covering 90°. The goniometer was used to precisely control the incident angle of the radiation. Data was gathered by rotating the crystal through 4° about the expected Bragg angle, calculated using the approximate d-spacing of the crystal, in 0.025° steps. After each 0.025° rotation a computer controlled shutter would open, exposing the stationary crystal for 0.5 seconds, with an uncertainty of 20 ms. Without the presence of a shutter the image plate would become saturated, causing the data to be inaccurate. The experimental setup is diagramed in Figure 7.

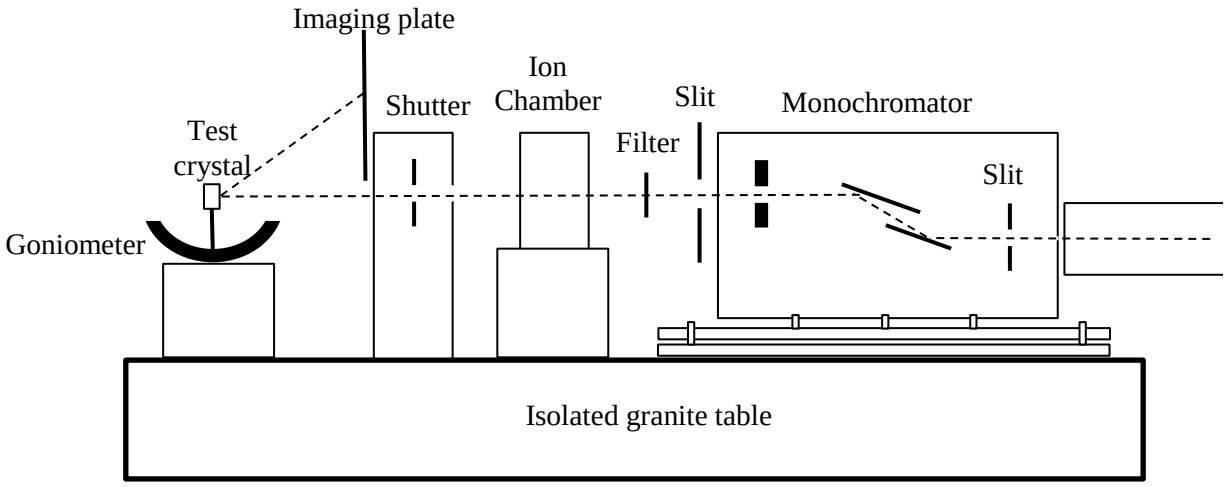

Figure 7. Schematic of experimental setup. Beam from the storage ring enters from the right.

Data was collected using imaging plates placed approximately normal to the reflected beam, as seen in Figure 8. The plates were read roughly 15 minutes after exposure. This delay was to avoid the sharp, non-linear drop in image plate signal occurring shortly after exposure. After this amount of time the signal on the image plates will decay in a linear manner, allowing for an easy adjustment to be made accounting for difference between read times.

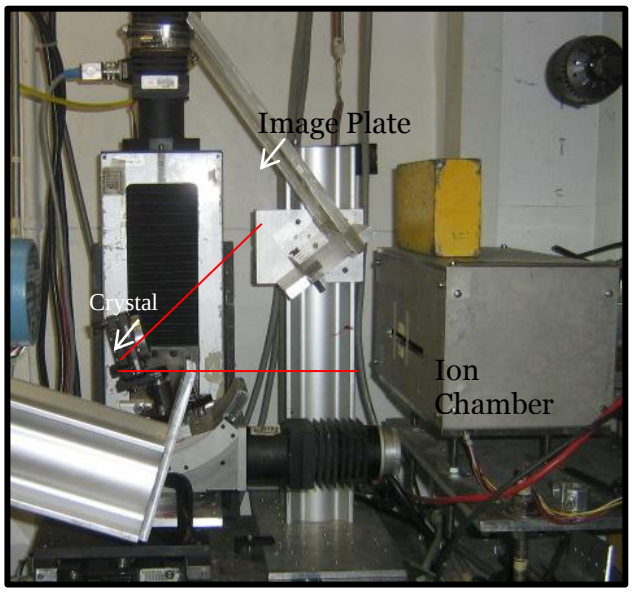

Figure 8. Photograph of crystal and image plate placement. The red line shows approximate beam path.

The yellow lead brick seen in Figure 8 was placed to shield the back of the image plate from stray radiation. Additional shielding was placed behind the plate which cannot be seen in this figure. For each of the four energies of interest multiple iterations of the entire angle sweep process were performed, as well as several which were slightly higher and lower than the roughly calculated Bragg angle.

Data

Figure 9. gives an example of the raw data obtained from the image plates. This data was gathered using a beam energy of 15.6909 corresponding to Zr $K\alpha_2$. The separate spots, similar to the pattern expected from single slit interference, are caused by the use of the shutter. The different shades seen on the image plate are caused by overlapping filters placed behind it. This background signal was accounted for in the analysis. The same image plate was repositioned and

used three times, causing the groupings of three rocking curves seen. The different groupings spread about the image plate are higher order (n>1) reflections.

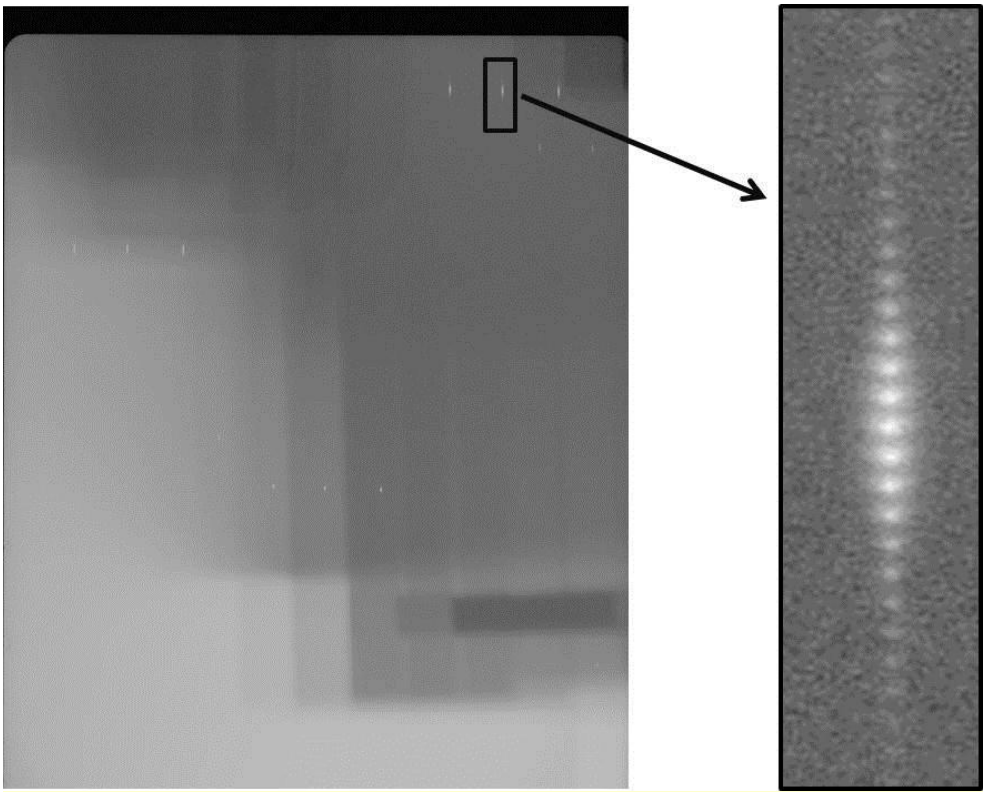

Figure 9 . Example of raw image plate data and enlarged n=1 reflection data for synchrotron x-ray energy corresponding to Zr $K\alpha_2$.

Analysis

Using Matlab the rocking curve was reconstructed using numerical interpolation, that is, using the data points gathered during each shutter opening for each angle calculating what the signal is expected to be during the angles in between each 0.025° step. A line out taken vertically through the center of the rocking curve was then fitted to a Gaussian. This Gaussian fit was used to

calculate the Rocking curve. Figure 10 shows an example of this process for the Zr $K\alpha_2$ energy. Figure 10. (a) is a false-colored image of the raw data for the rocking curve. Figure 10. (b) shows this raw data after the numerical interpolation has filled in the expected signal between shutter openings. Figure 10. (c) displays the lineout and Gaussian fit for the rocking curve.

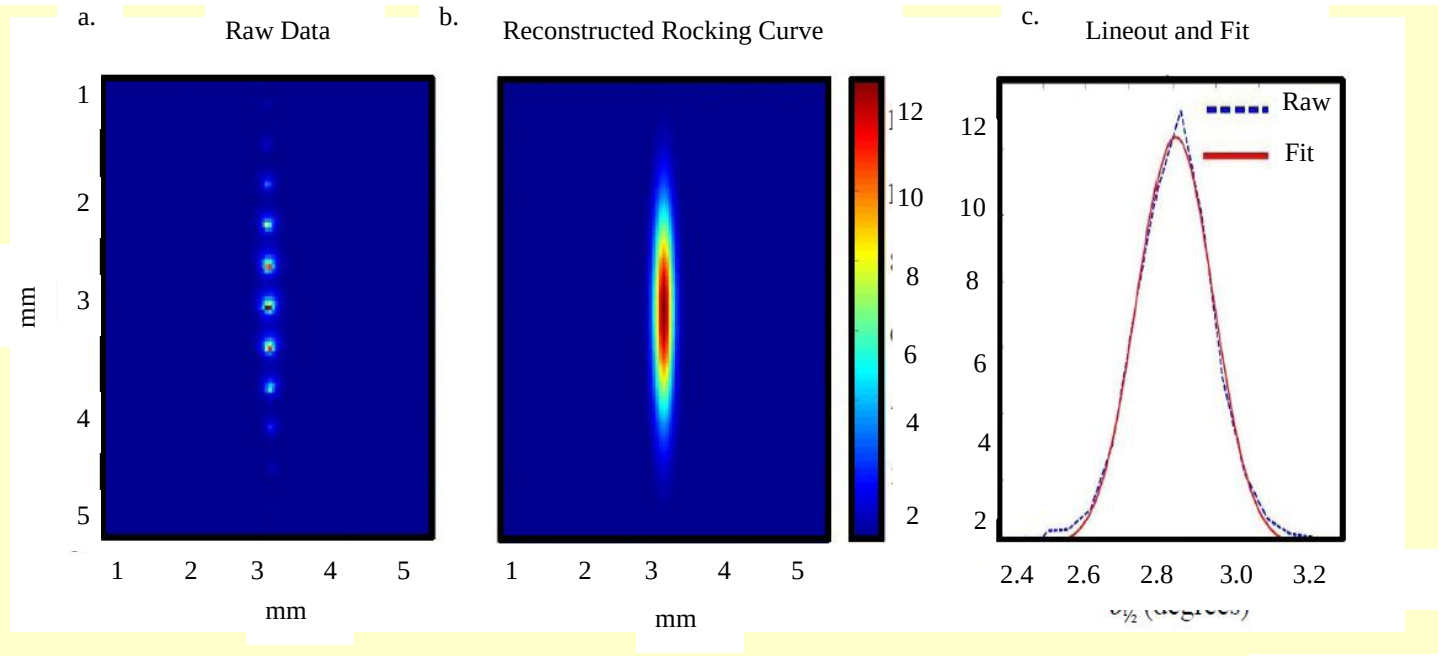

Figure 10. Rocking curve calculation for Zr Kα2. (a) False color image of a rocking curve such as that seen in Figure 9. (b) Rocking curve reconstructed using numerical interpolation. (c) Lineout taken vertically through the center of b.and fit with a Gaussian

The location of the peak of this curve corresponds to the Bragg angle and the Full-Width-Half-Maximum (FWHM) gives the rocking curve. Figure 11. displays the Gaussian fits for all four energies and their corresponding rocking curves.

The complement to the Bragg angle for Zr $K\alpha_2$ is 2.8°±0.12°, which can be used in conjunction with Bragg's Law to provide information about the d-spacing. The rocking curves for Zr $K_{\alpha 2}$, Nb $K_{\alpha 2}$, Mo $K_{\alpha 1}$ and Ag $K_{\alpha 2}$ are $0.42^o \pm 0.013^o$, $0.16^o \pm 0.02^o$, $014^o \pm 0.02^o$ and $0.17^o \pm 0.01^o$ respectively.

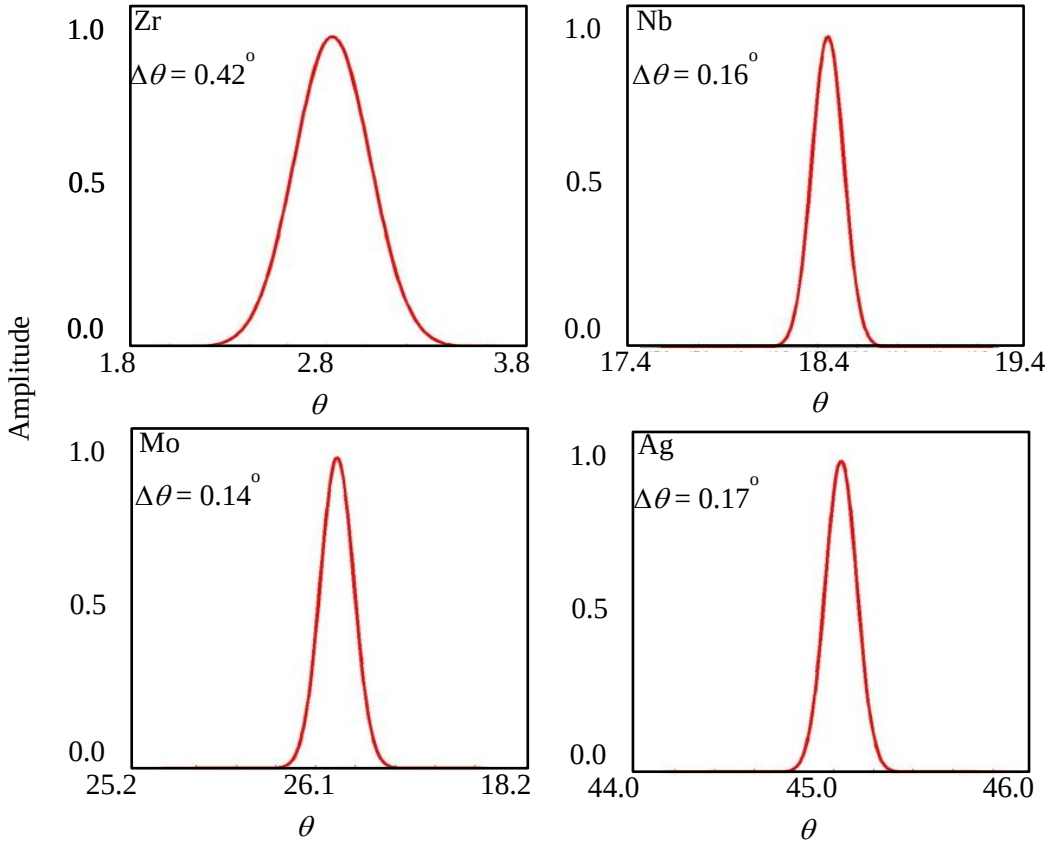

Figure 11. Examples of the Gaussian fit of the rocking curves for each of the four energies used and the corresponding rocking curve values.

The reflection efficiency was defined as the total x-ray energy reflected off of the crystal divided by the total energy incident on the crystal. Information about the total energy reflected off of the crystal was gathered from the data used to calculate the rocking curves. To calculate the total flux reaching the crystal control shots were taken. To accomplish this, an image plate was placed directly behind the ion chamber. Aluminum filters were used to prevent saturation of the image plate. There were several factors which had to be accounted for in calculating the flux. The different harmonics in the beam, the way the beam and its harmonics were attenuated when

passing through the Al filters, attenuation of the beam through air, the sensitivity of the imaging plates for the different energies, varying delay times before reading the image plates, and differences in the main beam current.

The monochromator will pass not only the selected energy, but also its harmonics. These harmonics are at energies which are multiples of the chosen energy. For example Zr Kα2 has an energy of 15.6909 keV so its third, fourth, and fifth harmonics have energies 47.0727 keV, 62.7636 keV, and 78.4545 keV respectively. Generally these harmonics are a relatively small percentage of the beam as seen in Table 1(a). However, the higher energy harmonics are attenuated less than those of lower energy, and so the balance of energies is changed as the beam passes through the 3.61 mm of Al filter. The percentages of the total flux consisting of each harmonic after the filter is shown in Table 1(b).

a. Unfiltered Beam

Harmonic	Percentage of Beam
1st	99.70%
3rd	0.28%
4th	0.01%
5th	0.00%

b. Beam in Al Filter

Harmonic	Percentage of Beam
1st	46.90%
3rd	50.40%
4th	2.60%
5th	0.06%

Table 1. a. The percentage of the unfiltered beam which is made up of each harmonic for Zr Kα2. b. Percentage of the beam which is made up of each harmonic after 3.61 mm of Al.

Using a table of mass attenuation coefficients [6], the attenuation coefficients for the specific energies of interest and their harmonics were interpolated. This coefficient describes the amount per unit mass that a substance, in this case Al, will absorb light of a specific wavelength. Using these coefficients the total signal on the image plate was adjusted to determine the flux of

the fundamental before passing through the Al. The image plate data post-crystal was also adjusted to account for attenuation of the fundamental while passing through the 54.3 cm of air between the ion chamber and the image plate.

The sensitivity of the imaging plates was found by comparing the flux of the beam through the ion chamber and comparing this to the signal on the image plate. This sensitivity was then accounted for in the total signals.

To account for varying delays between exposing the image plates and reading them, the average delay in seconds was found and the total signal normalized to this value.

The main beam current was linearly related to the flux of the x-rays. Therefore the signal was also normalized to account for variations in the current, which tended to decrease throughout the day.

With all of these factors taken into account the adjusted signal on the imaging plates taken after the beam was reflected off of the crystal was compared to the adjusted control shots and the reflection efficiency of the crystal was found. The results are shown in Table 2. These numbers were calculated to be accurate within a factor of two.

X-ray	Efficiency
Zr $K_{\alpha 2}$	4.2×10^{-5}
Nb $K_{\alpha 2}$	1.9×10^{-4}
Mo $K_{\alpha 1}$	5.5×10^{-5}
Ag $K_{\alpha 2}$	7.6×10^{-5}

Table 2. Reflection efficiency of the crystal for each of the four x-ray energies.

Further Experimentation

Once characterized, the crystal was used to image the Kα radiation from the rear surface of 17 μm thick Zr targets. This experiment was performed at the Laboratory for Laser Energetics at the University of Rochester. The multi-terawatt (MTW) laser was used, providing a 10 ps pulse and approximately 10 J of energy.

Several steps were taken to reduce background noise on the imaging plates used to gather the data. A 16 μm thick Zr filter was placed before the image plate. A 3 mm thick lead collimator was used to block radiation coming directly from the target chamber. Additionally the laser was defocused so that the focus on the target had a radius of approximately 10 μm, giving a mean intensity of 10^{17} W/cm^2. The crystal was aligned so that the incident angle was 2.8°, corresponding to the Bragg angle calculated in the earlier study.

The first ever image of Zr Kα x-rays was successfully obtained with a signal to background ratio of 40 to 1. This image is shown in Figure 12. alongside lineouts taken through the center of the image both horizontally and vertically.

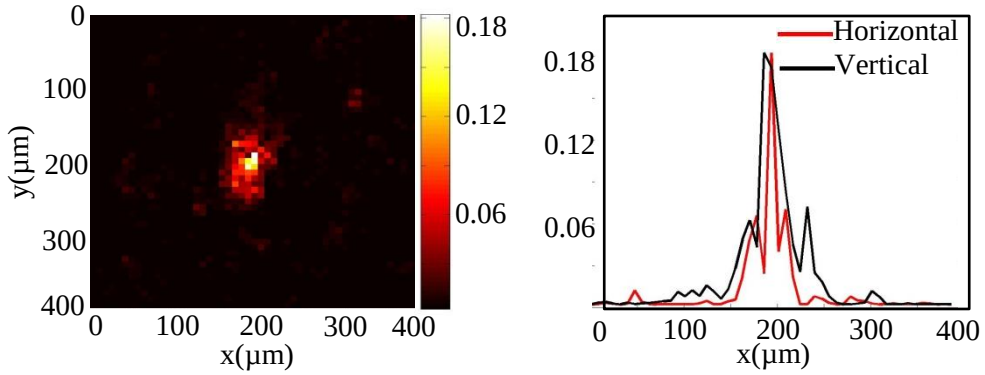

Figure 12. Image of Zr Kα obtained using the crystal during the MTW laser experiment. A lineout through the center of the image is shown taken in both the horizontal and vertical orientation.

A single photon counting spectrometer was used to determine the total number of Kα photons generated by the laser. Adjusting for attenuation in the filters and through air and for the image plate sensitivity the reflection efficiency of the crystal was found to be approximately $7x10^{-5}$. This is within the experimental error of the reflection efficiency previously found.

Conclusion

A spherically bent Bragg crystal x-ray imager which could image higher energy Kα than current crystals are capable of was desired. Such a crystal would be useful for a variety of experiments, and this crystal will be used in fluorescent layer experiments related to studies of the Fast Ignition scheme of direct drive laser fusion.

The quartz crystal was characterized for x-ray energies corresponding to Zr $K_{\alpha 2}$, Nb $K_{\alpha 2}$, Mo $K_{\alpha 1}$ and Ag $K_{\alpha 2}$. The rocking curves and reflection efficiencies for each energy were found.

Using this information the crystal was then used to obtain the first ever image of a Zr Kα emission. While the reflection efficiency may be too low for use in some experiments, this crystal will certainly be a useful diagnostic in many efforts.

References

[1] John Lindl, ”Development of the indirect-drive approach to inertial confinement fusion and the target physics basis for ignition and gain”, *Phys. Plasmas* **2**, 3933 (1995)

[2] John D. Lindl, Peter Amendt, Richard L. Berger, S. Gail Glendinning, Siegfried H. Glenzer et al. “The physics basis for ignition using indirect-drive targets on the National Ignition Facility”, *Phys. Plasmas* **11**, 339 (2004)

[3]Tabak, Max; Hammer, James; Glinsky, Michael E.; Kruer, William L.; Wilks, Scott C.;Woodworth, John; Campbell, E. Michael; Perry, Michael D.; Mason, Rodney J. “Ignition and High Gain With Ultra Powerful Lasers”, *Physics of Plasmas* **1**,1626-1634 (1994)

[4] “Introduction to fusion“, Culham Centre for Fusion Energy, 2009 <http://www.ccfe.ac.uk/introduction.aspx>

[5] “Inertial Fusion Energy”, Lawrence Livermore National Laboratory <https://lasers.llnl.gov/programs/ife/>

[6] J. H. Hubbell^{+} and S. M. Seltzer, “Tables of X-Ray Mass Attenuation Coefficients and Mass Energy-Absorption Coefficients from 1 keV to 20 MeV for Elements $Z = 1$ to 92 and 48 Additional Substances of Dosimetric Interest”, The National Institute of Standards and Technology, 1996, <http://www.nist.gov/pml/data/xraycoef/index.cfm>